# Experimental characterization of ID-Hall, a double-stage Hall thruster with an inductive ionization stage

**IEPC-2019-582**

*Presented at the 36th International Electric Propulsion Conference*
*University of Vienna • Vienna, Austria*
*September 15-20, 2019*

A. Martín Ortega[1], A. Guglielmi[2], F. Gaboriau[3] and J.P. Boeuf[4]
*LAPLACE, Université de Toulouse, CNRS, INPT, UPS, 118 Route de Narbonne, 31062 Toulouse, France*

*and*

C. Boniface[5]
*Centre National d'Etudes Spatiales (CNES), 18 avenue Edouard Belin, 31401, Toulouse, France*

**Abstract: We present experimental results on ID-Hall, a Double Stage Hall Thruster with an inductively coupled magnetized ionization stage. This first experimental prototype of ID-Hall operates in a low power regime, typically below 300-400 W. The purpose of this work is to study the properties of ID-Hall and provide directions for optimization, but also and more generally, to study the relevance of the double-stage concept and understand the specific properties of double-stage thrusters with respect to important physics issues such as current oscillations and anomalous electron transport. We present experimental measurements of the current voltage characteristics, extracted ion beam current (Faraday cup measurements), and ion energy and angular distribution functions (RPA measurements) in a single stage and double stage regime of operation, as a function of DC voltage and RF power. The results demonstrate that ions can be extracted from the inductive RF ionization stage even under conditions where the applied DC voltage is not sufficient to ionize the gas flow, i.e. that ID-Hall can indeed operate in a double stage regime.**

## I. Introduction

IN Double Stage Hall Thrusters (DSHTs), a separate ionization source is placed upstream of the magnetic barrier in order to allow separate control of thrust (i.e. ionization) and specific impulse (i.e. ion acceleration). The concept of DSHT could also be useful for operation of the thruster with alternative propellants more difficult to ionize than xenon (krypton, argon, air breathing thrusters). A variety of double stage Hall thruster designs have been proposed[1-10] but the relevance of the concept has not really been demonstrated[11]. The ion extraction area of a Hall thruster is much smaller than that of a gridded thruster so that efficient confinement of the plasma in the ionization stage and plasma generation as close as possible to the acceleration region are essential aspects of an efficient DSHT (the

[1] Research engineer, IRT Saint-Exupéry, martin-ortega@laplace.univ-tlse.fr
[2] PhD Student, Univ. Toulouse, guglielmi@laplace.univ-tlse.fr
[3] Associate Professor, Univ. Toulouse, freddy.gaboriau@laplace.univ-tlse.fr
[4] Directeur de Recherche CNRS, jpb@laplace.univ-tlse.fr.
[5] Electric propulsion R&T manager, CNES, French Space Agency, claude.boniface@cnes.fr

effective wall loss area in the ionization stage, taking into account magnetic confinement, should be small with respect to the channel extraction area). We have recently introduced a new design of DSHT, called ID-Hall[11-13] (for **I**nductively coupled **D**ouble stage **Hall** thruster, patent pending) where the ionization stage is a magnetized RF inductively coupled plasma source with an RF coil inside the inner cylinder of the thruster (Figure 1). The dimensions of the first experimental prototype of ID-Hall described here are such that the thruster can operate at a total power below 300-400 W. In this paper we present an experimental characterization of ID-Hall operating in single stage and double stage regimes. Measured thruster characteristic as a function of DC voltage in the acceleration stage and RF power in the ionization stage, including V-I curves, Faraday cup measurements of the extracted ion current and RPA measurements of the ion energy distribution function are discussed below. The ID-Hall design is briefly described in section II. The experimental set-up and diagnostics are presented in section III, and the main results are discussed in section IV.

## II.ID-Hall design

The characteristic feature of the ID-Hall thruster is the RF inductively coupled plasma source placed inside the central cylinder of the thruster. In this configuration, the ionization source is close to the magnetic barrier, so that the ionization chamber is just an extension of the thruster channel. For this prototype the coil was 25 mm long and 20 mm in diameter, with 11 turns around a ceramic holder[12]. A low-loss ferrite of 10 mm diameter is placed at the center of the coil to act as a magnetic conductor for both the DC field creating the magnetic barrier and the RF field of the inductive source. Two ferrite discs of 22 mm diameter are placed on both extremities of the inductive coil, with 1-mm thick samarium-cobalt (SmCo) magnets placed around the ferrite discs, the magnetization being in the radial direction. The assembly of the inductive coil, ferrite and magnets is contained inside a 26-mm diameter Pyrex tube which also acts as the inner insulating wall of the thruster. The outer wall is made of alumina and has two distinct regions: a cylindrical part of 46 mm diameter and 10 mm length and a conical-shaped wall that extends from the 46 mm cylinder diameter to 92 mm diameter over a length of 30 mm. Two sets of SmCo magnets are placed immediately behind the channel wall and at the end of the conical wall. Both sets of magnets are kept in place by an L-shaped soft iron piece; this piece also closes the DC magnetic circuit. The combination of the conical wall and the placement of the magnets creates an ionization chamber with 4 magnetic cusps and magnetic field lines parallel to the walls, reducing the ion losses at the walls and increasing the plasma density. In addition to the magnetic barrier of the thruster channel, a second magnetic barrier is created at the base of the ionization chamber. A schematic of the ID-Hall design is shown in Figure 1. The magnetic field configuration of the ID-Hall prototype is slightly different from that used for previous simulations[11], due to the use of ferrites in the RF source instead of soft iron. The ferrites have a lower saturation field than soft iron (500 mT vs. 2 T respectively); as a consequence, the field lines are no longer parallel to the inner wall and a region of weak magnetic field appears instead close to the inner wall.

The expected effect is a less efficient confinement of the plasma and a larger loss of ions to the inner wall. The zero magnetic field point should be moved radially away from the inner cylinder in future prototypes.

The anode consists of a copper disc of 40 mm diameter and 4 mm width, covered on the back side and on the inner and outer diameters by an insulating ceramic, so that only the front side of the disc is exposed to the plasma. It is placed at the maximum of the second magnetic barrier, so that the surface of the disc is approximately parallel to the magnetic field lines. Xenon is injected at the base of the ionization chamber after passing through a disc of porous ceramics. The cathode used in this study was provided by ICARE[14]. It is a hollow cathode with a $LaB_6$ disc placed behind the aperture and heated by a 200 W tungsten filament. A starter is used to trigger the discharge but is not required during continuous operation of the thruster.

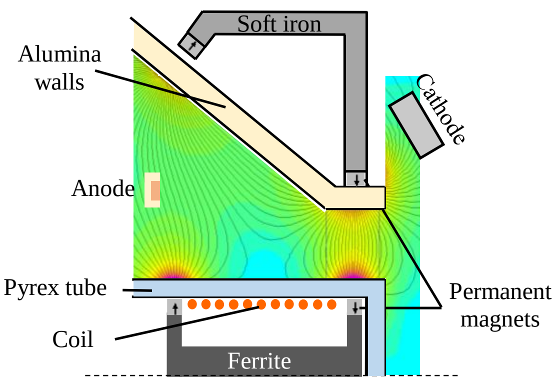


**Figure 1. Schematic of the ID-Hall thruster prototype used in this study showing the magnetic field lines and intensity.**

The RF power source is an RFG 50-600 from Coaxial Power Systems operating at 4 MHz. The reduced frequency (with respect to the standard 13.56 MHz) was chosen to reduce the capacitive coupling and the losses in the central ferrite; a side-effect is the increase of the current and the ohmic losses[15].

## III.Experimental apparatus and procedure

### A. Setup and experimental conditions

The ID-Hall thruster is fixed at one end of a vacuum vessel of 1 m length and 0.5 m diameter (former GREMI vacuum vessel[16]). The vessel is equipped with three turbo-molecular pumps providing a total pumping speed of 4200 l/s. Quartz windows at the other end and at one side of the vessel provide frontal and lateral views of the thruster in operation. All measurements presented here were performed with a Xe flow rate of 6 sccm through the anode, and 1.5 sccm through the cathode; under these conditions the pressure in the vessel reached $6{\cdot}10^{-5}$ mbar.

The ensemble of anode, cathode and starter/keeper together with their power sources floated with respect to the grounded chamber walls. The discharge current was obtained by measuring the voltage drop across a test resistance of 1.8 Ω in the anode side, by means of a differential probe and a digital oscilloscope. As a redundancy, a Rogowsky coil also measured the discharge current oscillations. The potential difference between cathode and ground was measured using a digital multimeter.

### B. Faraday probe measurements

The Faraday probe used in this study consisted in two collector discs of 25 mm diameter on opposite sides of the probe, each one surrounded by a guard ring of 2 mm width. The Faraday probe is mounted on a rotating arm of 225 mm length and can reach angles from +80 degrees to -45 degrees, taking the thruster symmetry axis as the angular reference. The arm is connected to an in-vacuum stepper motor and rotating assembly which allows angular steps as small as 0.5 degrees. An automatic control and acquisition system designed and built at LAPLACE allowed automatic angular scans with variable angular steps, recording of the value of the angle and the current collected from both front and rear collector surfaces at each step. During the measurements the collectors and guard rings were biased to -40 V to repel the background electrons. A diagram of the control and acquisition system is shown in Figure 2.

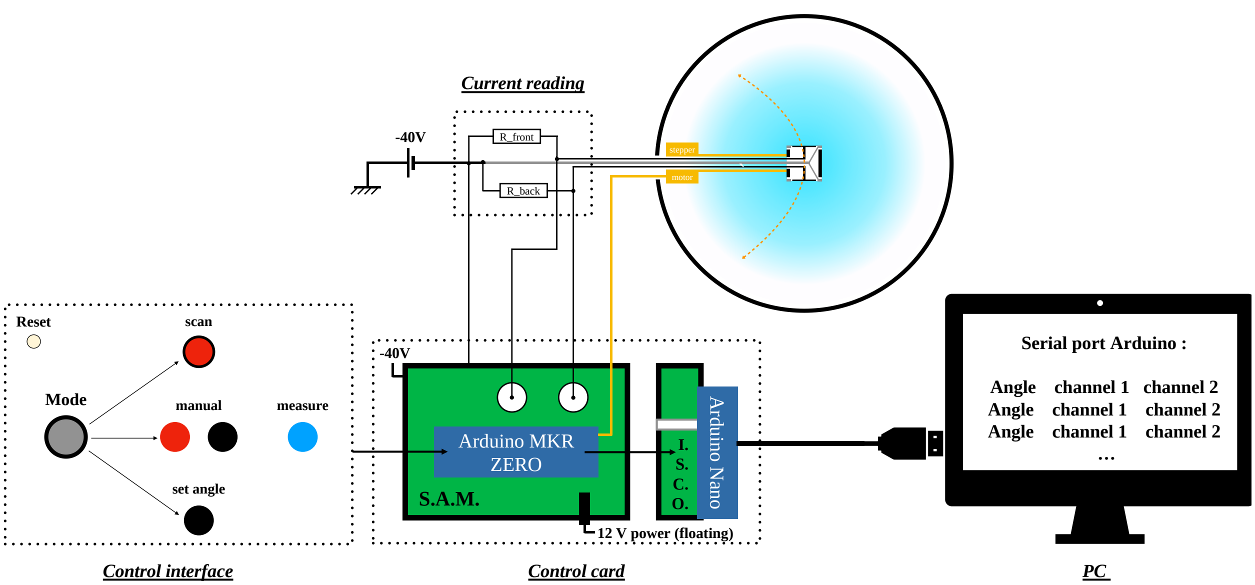


**Figure 2. Schematic of the Faraday probe automatic acquisition system**

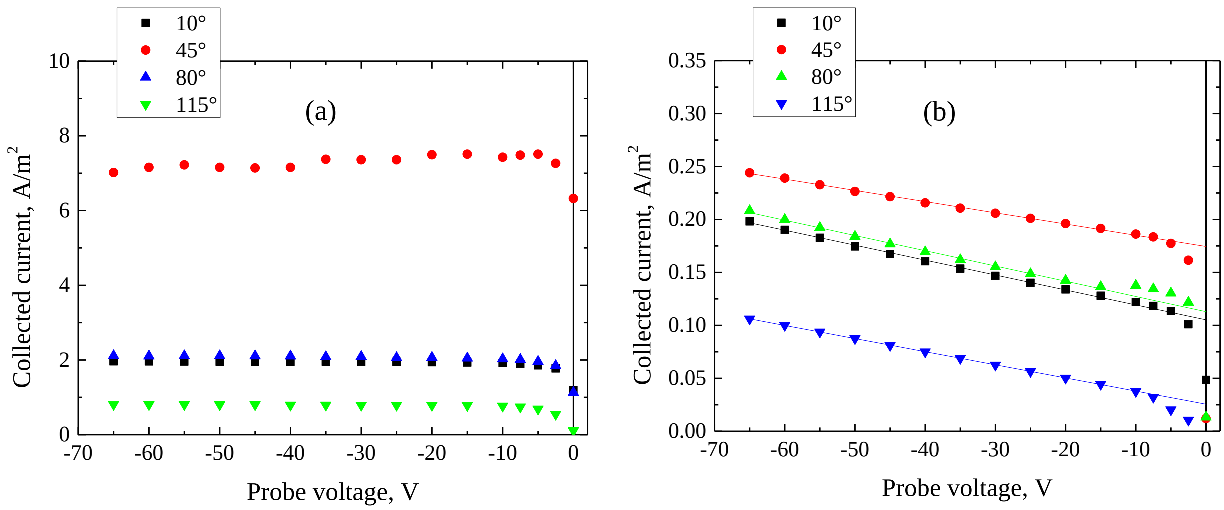


**Figure 3. (a) Current at the front collector of the Faraday probe as a function of probe voltage for different angles. (b) Current at the back collector of the Faraday probe as a function of probe voltage for different angles (symbols). Lines: linear fit of the points for V≤-10 V.**

The current collected from the back collector is used to calculate the contribution of the background plasma and is subtracted from the current measured by the front collector. However, while the current in the front collector is independent of the probe voltage once the electrons are repelled (V<-5 V, Figure 3a), the sheath expansion on the back side leads to a continuous increase of the collected current as a function of the bias potential[17] as can be seen in Figure 3b. To account for the sheath expansion, a number of I-V curves were taken at several angular positions; the ion current corresponding to the collector surface was taken as the extrapolation to 0 V of a linear fitting of the measured I-V curves. The fitting coefficients obtained were used later to obtain the background current from measurements at the fixed probe bias of -40 V.

Once the angular distribution of the ion current is known, the total ion current can be calculated as

$$I_i = 2\pi R \int_0^{\pi/2} J_i(\theta)\sin(\theta)d\theta$$

where $J_i$ is the ion current density, $\theta$ the azimuthal angle and $R$ the distance from the probe to the thruster, coincident with the probe rotation axis. In practice, the integral is not calculated up to $\pi/2$ but only to the largest available angle, i.e. +80 degrees. However, we expect this to be a good approximation to the true ion current, and in any case it will allow to examine the variations of ion current as a function of the different operating conditions. Also, given the relatively high background pressure, we expect the ion current at large angles to be highly overestimated due to charge-exchange collisions (CEX)[18], so that the measurements at higher angles would not be representative of the true plume ion current in vacuum.

### C. RPA measurements

The RPA used in this study has a standard 4-grid analyzer design and is placed on a rotating arm, capable of measuring at ±30 degrees[19]. We measured the IEDF only at the centerline, the angular distributions of ion current being already recorded by the Faraday probe. The RPA was placed 55 cm away from the thruster. The rejecting grid voltages were set to -35 V and -40 V to prevent respectively external electrons from entering the RPA and secondary electrons from being emitted away from the collector surface. The voltage of the analyzer grid was proportional to the voltage of a function generator providing a triangular signal, the upper and lower limits of the sweeping voltage being adjusted at each operating condition to obtain the best energy resolution possible. The frequency of the generator voltage was around 500 Hz, much lower than any oscillation observed in the discharge current. Both analyzing voltage and RPA signal were recorded using a digital oscilloscope. The derivative of the recorded signal with respect to the voltage was obtained using a Savitzky-Golay filter to obtain the IEDF of the ions.

## D. I-V probe and RF source efficiency

The efficiency of the inductive RF source was measured using a current-voltage probe connected to a digital oscilloscope. First, the RMS current and voltage were measured without plasma; in this configuration the power loss is due to ohmic dissipation in the copper wire and to magnetic losses in the ferrite core. Assuming that all the power losses are due to ohmic heating, the resistance can be calculated as $R_{wire} = P/I_{RMS}^2$, where $P$ is the injected power measured by the RF source and $I_{RMS}$ is the root mean square of the RF current. The resistance was found to be $R_{wire}=2.5$ Ω. Then, the power coupled to the plasma will be the difference between the injected power and the heating losses: $P_{plasma} = P_{tot} - R_{wire}I_{RMS}^2$.

# IV.Results and discussion

## A. Single stage characterization

ID-Hall was first characterized in single-stage operation, i.e. without power in the inductive plasma source, at an anode flow rate of 6 sccm and a cathode flow rate of 1.5 sccm (0.6 mg/s anode and 0.15 mg/s cathode).

To verify the reproducibility of the results, several voltage sweeps were performed at different times (Figure 4): right after the starting of the discharge ("cold"), after a few minutes of operation ("warm") and finally and the end of the measurements ("hot"). In addition to these sweeps, the angular ion current distribution and the IEDF were measured every 10 V, together with the discharge current waveform. There were some variations of the discharge current between the different sweeps, but the general features were well reproduced in all three cases. One can distinguish two distinct discharge regions: a first region below 190 V, where the discharge current passes through a maximum around 0.68 A and decreases slowly to 0.58 A with increasing voltage, and a second region above 190 V where the current increases continuously with increasing voltage. This continuous increase at higher voltages is thought to be caused by secondary electron emission from the alumina walls and is consistent with previous observations[20] of Hall thruster I-V characteristics with alumina walls. This is in contrast with the I-V characteristics of Hall thrusters with BN or BN-$SiO_2$ walls which exhibit a long region of constant current above 150 V[20]. The current oscillations below and above 190 V are also very different, as can be seen in Figure 5. Breathing oscillations are observed below 190 V, with a well-defined frequency increasing from 8 kHz at 100 V up to 15 kHz at 180 V. The amplitude of the oscillations (Figure 5), is between 2 and 3 times the mean current in this part of the I-V characteristics. At higher voltages the breathing mode oscillations disappear, and the random fluctuations of the current have much smaller amplitudes. We call this regime "continuous mode". Details on the dynamic behavior of the breathing mode can be found in the companion paper[21].

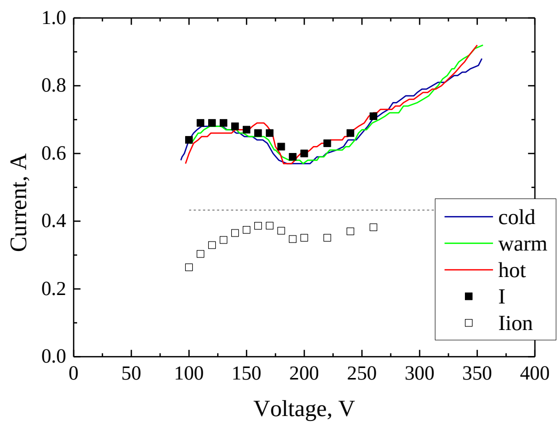


**Figure 4. Lines: I-V sweeps performed just after initiation of the discharge ("cold"), after 5 minutes of operation ("warm") and after two hours ("hot"). Open square symbols: discharge current measured simultaneously with the Faraday probe scans. The dashed line corresponds to the maximum $Xe^+$ ion current at 6 sccm.**

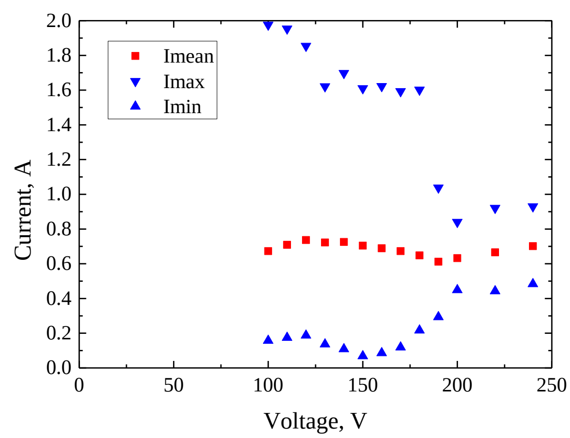


**Figure 5. Mean discharge current (square symbols) and maxima (down triangle symbols) and minima (up triangle symbols) of the oscillations as a function of the discharge voltage in single stage operation. Large amplitude "breathing mode oscillations" are present below 190 V while a quasi "continuous mode" exists above 190 V.**

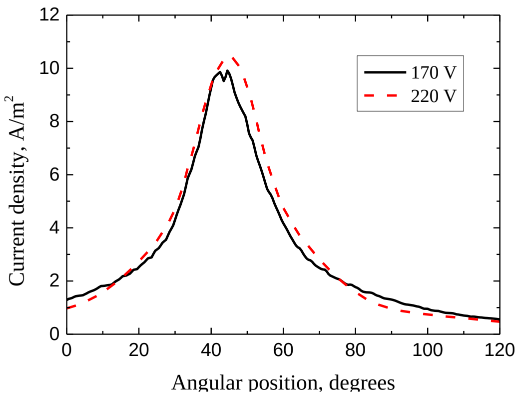


**Figure 6: Angular distribution of the ion current in the plume in single stage operation, with (170 V) or without (220 V) the presence of breathing mode oscillations in the discharge current.**

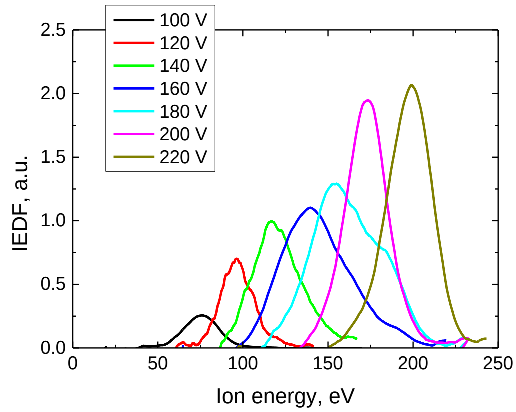


**Figure 7: IEDF measured by RPA at the symmetry axis of the thruster for different discharge voltages, in single stage operation.**

The results obtained with the Faraday probe (Figure 4) show that the ion current increases with voltage up to a maximum of 0.39 A at 170 V (the maximum $Xe^+$ current at 6 sccm is 0.43 A). Above this voltage, the ion current drops together with the total current, then slightly increases as the voltage increases further. These differences come from differences on the ion current at large angles; the angular distributions (Figure 6) have a similar maximum ion current and vary only slightly at large angles. The divergence angle, taken as the half-angle which contains 90% of the ion current, is also similar: for the two distributions of Figure 6, it is 65 degrees at 170 V and 63 degrees at 220 V.

Finally, the RPA measurements show two distinct IEDF profiles depending on whether breathing oscillations are present or not, as shown in Figure 7. In the oscillatory mode, the IEDF has a larger width, with the peak being slightly lower than the discharge voltage. Above 180 V, in the continuous mode, the distributions become much narrower, again with the maxima being lower than the corresponding discharge voltage. The energy shift between the peak of the distribution and the discharge voltage is not due to the cathode potential, which was measured simultaneously and found to be only of around -5 V, while the difference between the maxima and the discharge voltage is about 20 V. This difference may be due to the presence of a second magnetic barrier in the anode region at the end of the ionization stage of ID-Hall. Under some conditions, a potential drop may form in this region because of the smaller electron mobility, leading to a plasma potential lower than the anode potential and lower maximum ion energy at exhaust. The presence of such potential drop in the anode region in single stage operation has been predicted by the hybrid model HALLIS[11, 22]. Time resolved RPA measurements presented in the companion paper[21] show that the larger width of the IEDF that can be seen in Figure 7 for discharge voltages below 200 V is actually due to an oscillation of the plasma potential with respect to the anode potential when breathing oscillations are present.

## B. Double stage characterization

To characterize the effect of the double stage operation of ID-Hall, we performed both sweeps of the injected RF power at fixed discharge voltage, and voltage sweeps at fixed injected RF power. During the power sweeps, the voltage was fixed from 0 V to 200 V every 50 V and the total current, ion current, IEDF distribution and source efficiency were measured every 10 W of injected RF power. These sweeps started at 0 W when the voltage is 100 V or above, i.e. at voltages where single stage operation was possible. At lower voltages, when single-stage operation was not possible, the sweeps started at the minimum RF power capable of sustaining the discharge. During the voltage sweeps, the power was fixed at 50 W, 100 W and 150 W, with measurements every 10 V. The minimum operating voltage was 0 V at 100 W and 150 W of injected power; at 50 W the minimum voltage was 60 V. The flow rates were as in the single-stage characterization, 6 sccm at the anode and 1.5 sccm at the cathode.

The RF power coupling efficiency of the plasma source, calculated as indicated in section III.D, is plotted in Figure 8 as a function of injected power (given by the RF power supply). We see that the power coupling efficiency of the RF source is close to 75% when the plasma density is high enough, i.e. at large RF power or large DC voltages. The power coupling efficiency of ICPs can be optimized to high values, larger than 90% (see, e.g., Ref. [23]) and optimization of the power transfer efficiency of the ionization stage of ID-Hall will be performed in future work. The results below are plotted as a function of injected power or absorbed power.

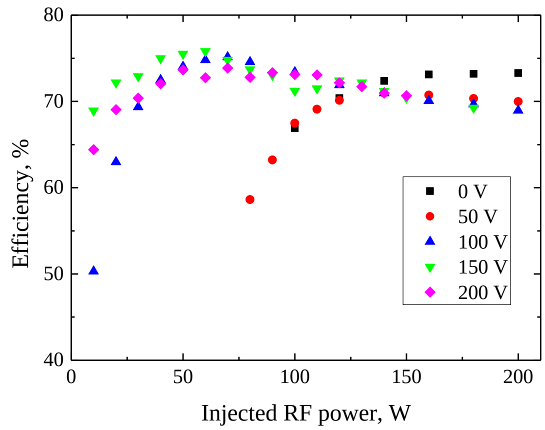


**Figure 8. RF source efficiency as a function of the injected power, for different values of the discharge voltage.**

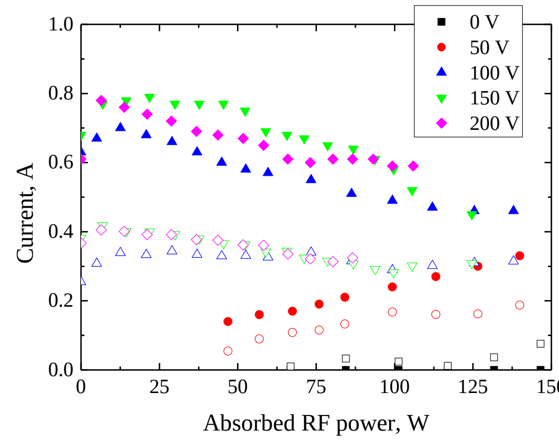


**Figure 9. Discharge current (full symbols) and ion current (open symbols) as a function of absorbed RF power, for different discharge voltages.**

Figure 9 shows the total discharge current and extracted ion current as a function of the absorbed RF power, for the 5 discharge voltages considered. At low voltages (0 and 50 V), both discharge current and ion current increase steadily with the applied power. Note that these voltages are too low to allow sufficient ionization by electrons coming from the cathode and the ions extracted from the thruster must have been generated in the ionization stage. This illustrates that ID-Hall can effectively operate in a double stage mode, with the ionization stage separated from the acceleration stage. There was no saturation of the ion current with increasing RF absorbed power up to 140 W, which means that a power higher than 140 W is required to fully ionize the gas flow at 50 V of discharge voltage. At higher voltages, the main effect of the RF power is the reduction of the total discharge current. For instance, at 150 V the current decreases from 0.68 A at 0 W to 0.45 A at 125 W (coupled power). The ion current also decreases with increasing power, but in a less pronounced way. For example, for a discharge voltage of 100 V, the total current decreases with increasing absorbed power above 15 W, while the measured ion current does not significantly decrease. This indicates that the electron current entering the thruster channel decreases with increasing RF power and suggests that anomalous electron transport in the channel is modified (and decreases) when the RF power absorbed in the ionization stage increases.

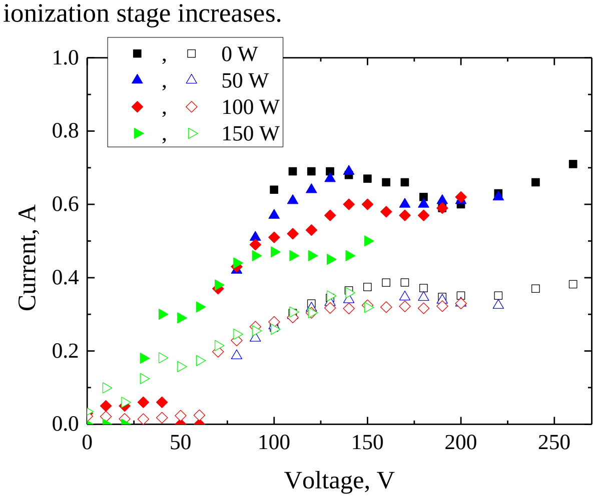


**Figure 10. I-V characteristics for different fixed RF injected power. Full symbols: discharge current. Open symbols: ion current.**

The influence of double stage operation on electron transport can be more clearly seen in Figure 10, which displays the I-V characteristics for different values of the RF injected power. For discharge voltages between 100 and 150 V, the total discharge current decreases clearly with increasing RF power, while the ion current does not significantly change. For discharge voltages below 100 V, the thruster cannot operate in single stage, but ions can be extracted from the ionization stage for large enough RF power. The ionization cost or discharge loss of the ionization stage, defined as the RF power divided by the ion beam current, is however very large, e.g. on the order of 150W/0.2A=750 eV/ion at 50 V, 150 W. The magnetic confinement in the ionization chamber must be optimized to improve the performance of the ionization stage. For voltages above 150 V and for this gas flow rate, operating in double stage is not useful since the discharge current and extracted ion current do not significantly change with RF power.

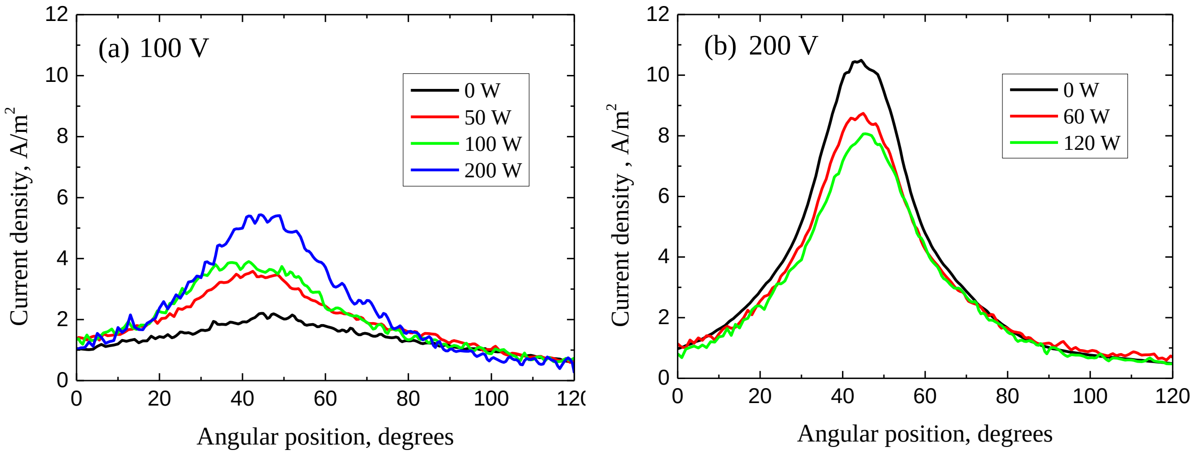


**Figure 11. Angular distributions of the ion current for different values of the RF injected power, (a), for a discharge voltage of 100 V, and (b), for a discharge voltage of 200 V.**

Figure 11 shows the angular distribution of the ion beam for two values of the discharge voltage (100 V in Figure 11a, and 200 V in Figure 11b) and for different values of the RF power. For a 100 V discharge voltage the beam divergence decreases with increasing RF power. This decrease of the divergence with increasing power can be attributed to the fact that ions are generated deeper in the ionization stage for larger RF power. Note that in this particular case the current at large angle is quite high and remains unchanged for all RF power. The contribution of the ion current at large angle to the total ion current is dominant so that the ion current does not change significantly with RF power (Figure 10) in spite of the lower divergence at higher RF power. For a discharge voltage of 200 V (Figure 11b), the observed trend is opposite, i.e. the ion beam divergence increases with increasing RF power (also without significant changes of the total ion current). This feature is not clearly understood.

We now look at the IEDF in double stage operation. Figure 12 shows the influence of the RF power on the IEDF for two different values of the discharge voltage. Interestingly, the energy of the ion beam is dependent on the RF power, and this clearly appears at low discharge voltages.

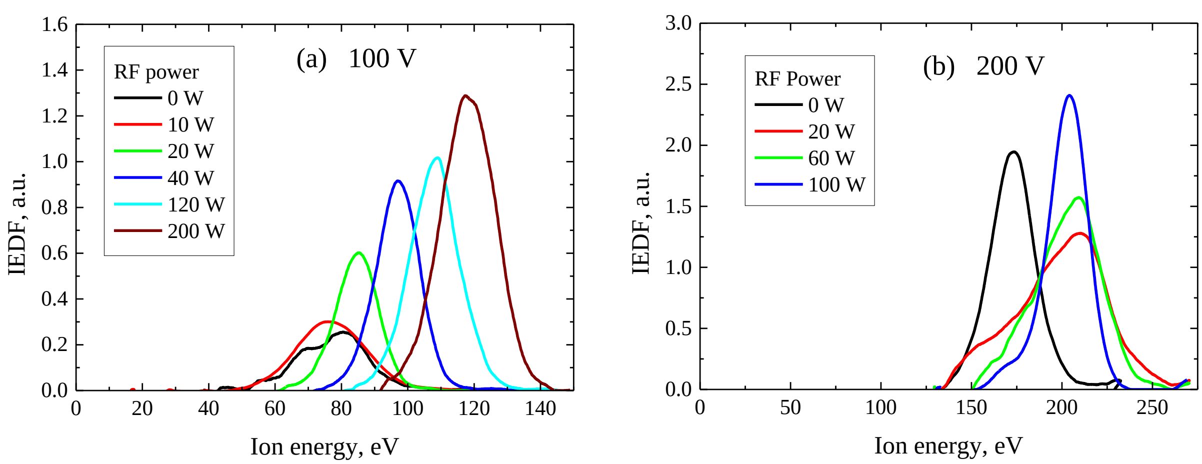


**Figure 12. IEDF for different values of the RF injected power and for two values of the discharge voltage, (a) 100 V, and (b) 200 V.**

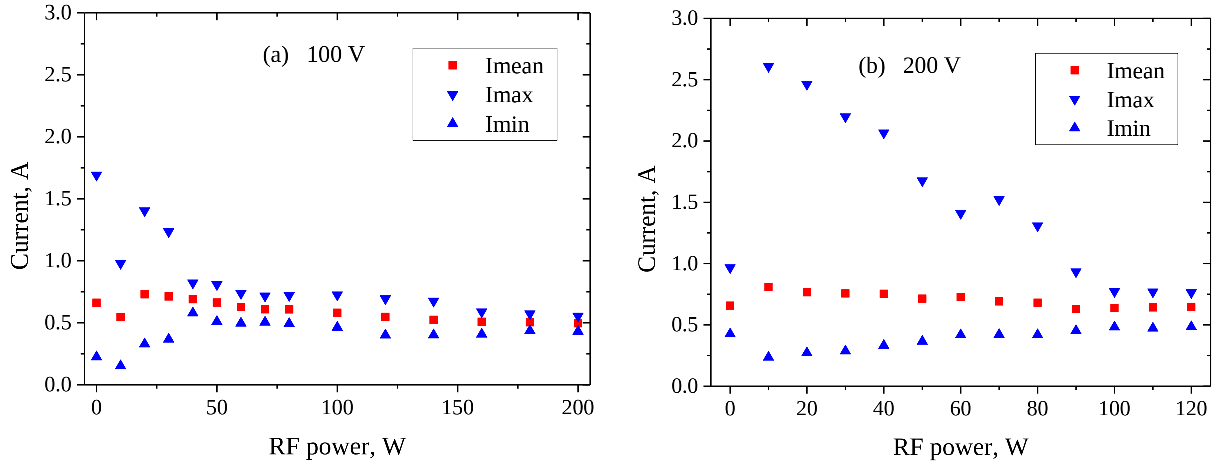


**Figure 13: Mean discharge current (squares), maxima and minima of the oscillations (up and down triangle symbols respectively) as a function of the RF power for a discharge voltage of a) 100 V and b) 200 V**

For a discharge voltage of 100 V (Figure 12a) the energy at the maximum of the IEDF increases with increasing RF power. The energy at the IEDF maximum is 75 eV at 0 W (single-stage) and increases gradually up to 120 eV at 200 W of injected RF power (138 W absorbed power). This energy is actually higher than the discharge voltage, which means that the ions are generated in a region at a potential higher than the anode potential. This suggests that the plasma potential in the ionization chamber is higher than the anode potential and increases with increasing RF power at a given discharge voltage. A possible explanation of this feature is that the electron mean energy in the chamber increases with the RF power. The electron temperature in a low-pressure plasma source at constant gas density depends mainly on the surface to volume ratio of the chamber (this results from the balance between ionization and losses), and not on the absorbed power. In our conditions we expect the gas density to be strongly depleted by ionization when the RF power increases and the ionization rate (and mean electron energy) should therefore increase with RF power. The plasma potential with respect to the walls in a low temperature plasma source is $T_e \ln\left(\frac{M}{2\pi m}\right)$, i.e. about $5.8T_e$ for xenon, with $T_e$ expressed in eV. For an electron temperature on the order of 5-6 eV, the plasma potential can be more than 30 V above the anode potential which is consistent with the results of Figure 12a.

At higher voltage (200 V, Figure 12b), the mean energy shifts from 181 eV at 0 W to 203 eV at RF powers above 40 W, which may also be attributed to an increase of the electron temperature in the ionization chamber. The profile of the IEDF is also affected by the RF power and changes from a well-defined narrow peak at 0 W to a broader distribution at low RF power. The width of the energy distribution becomes again narrower as the RF power increases.

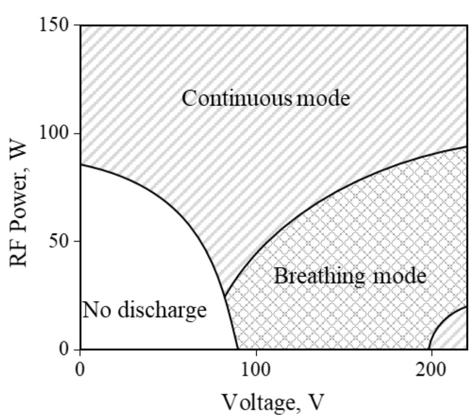


**Figure 14: Schematic diagram of the different regimes of ID-Hall.**

This effect is associated with the presence or absence of breathing oscillations (Figure 13). At the lower discharge voltage of 100 V (Figure 13a) breathing oscillations of moderate amplitude are present for RF power below 50 W, and disappear above 50 W. At the larger discharge voltage of 200 V (Figure 13b) very large amplitude breathing oscillations are present for RF power between 10 W and 100 W and much smaller amplitude current fluctuations are seen above 100 W. As in the single stage case of section IV.A, Figure 7, and as shown in the time-resolved RPA measurement of our companion paper[21] the larger width of the IEDF is due the presence of oscillations of the plasma potential with respect to the anode potential when breathing oscillations are present.

The domains of breathing oscillations (“breathing mode”) and small amplitude current fluctuations (“continuous mode”) are summarized in Figure 14. Note that the small region above 200 V at 0 W is also a “continuous mode”

## V.Conclusions

A prototype of the ID-Hall thruster has been built and tested at the LAPLACE laboratory. This first experimental prototype of ID-Hall has been characterized by measurements of the discharge current, Faraday probe measurements of the angular distribution of the ion current and RPA measurements of the ion energy distribution function.

In single stage operation, i.e. without power in the inductive RF plasma source, strong breathing oscillations are present below 190 V ("breathing mode") while only small amplitude current fluctuations are present above 190 V ("continuous mode"). The width of the IEDF is larger in the oscillatory mode than in the small amplitude fluctuating current mode. In both cases the maximum of the IEDF was lower than the applied voltage, the difference corresponding to a potential drop in the second magnetic barrier in front of the anode (this potential drop oscillates when breathing oscillations are present, leading to a wider IEDF).

In double stage operation it was possible to sustain a discharge at voltages that are too low for single stage operation; in these cases, the ionization and acceleration are effectively decoupled, proving that ID-Hall can actually operate as a true double stage Hall thruster. At intermediate voltages, between 100 V and 200 V, a region where the I-V characteristics of most single-stage Hall thrusters present an overshoot in the current (larger electron current due to a larger anomalous or collisional electron transport?), it is interesting to note that operating in a double-stage regime leads to a significant decrease of the discharge current while the extracted ion current remains unchanged. This suggests that operation in a double-stage regime significantly modifies electron transport in the channel. The breathing mode oscillations that appeared in single stage operations tended to disappear at high enough RF power in double stage operation. Divergence also decreases as the RF power increases at those intermediate voltages. Finally, the IEDF in double stage shows an increase of the ion energy with RF power; this increase is especially evident at low voltage, when the ion energy increases regularly with the absorbed RF power well beyond the applied voltage. This increase is a consequence of the plasma potential inside the ionization chamber increasing with RF power due to an increasing electron temperature with RF power.

These results show that that the possibility of operating in double stage is especially interesting for the use of propellants with lower atomic mass and/or less efficient ionization than xenon because 1) the same specific impulse (ion velocity) as in xenon will be obtained for lower applied voltages if the gas is lighter than xenon, and 2) supplementary ionization would be necessary in these conditions. Operation of ID-Hall in these conditions will be explored in future work. Optimization of the magnetic confinement in the ionization chamber and of the ICP power coupling will also be sought. Finally, double stage operation may also be useful at higher flow rates, if ionization by electrons coming from the cathode is no longer sufficient. We have not yet explored these conditions because of the limitations of our vacuum chamber and pumping facility.

## VI.Acknowledgments

This work is supported by CNES, the French Space Agency, and by the RTRA STAE foundation under the project INNPULSE. A. Guglielmi benefits for a PhD fellowship from CNES and Région Occitanie.

## VII.References

[1] Y. Peterson, PhD thesis, Michigan State University, 2004.

[2] A. I. Bugrova, A. V. Desiatskov, V. K. Kharchenikov, A. I. Morozov, and M. Prioul, in *29th International Electric Propulsion Conference, Princeton, NJ,* IEPC 2005-146, 2005).

[3] A. I. Morozov, A. I. Bugrova, A. V. Desyatskov, V. K. Kharchenikov, M. Prioul, and L. Jolivet, in *28th International Electric Propulsion COnference*, IEPC-2003-290, (Toulouse, France, 2003).

[4] C. Boniface, G. Hagelaar, L. Garrigues, J. P. Boeuf, and M. Prioul, IEEE Trans. Plasma Sci. 33, 522 (2005).

[5] L. Garrigues, C. Boniface, G. J. M. Hagelaar, and J. P. Boeuf, Phys. Plasmas 15, 113502 (2008).

[6] R. A. Martinez, W. A. Hoskins, P. Y. Peterson, and D. R. Massey, in *31st International Electric Propulsion Conference* (Ann Harbor, Mi, 2009), p. IEPC.

[7] H. Kuwano, A. Ohno, H. Kuninaka, and H. Nakashima, in *30th International Electric Propulsion Conference*, IEPC-2007-085, (Florence, Italy, 2007).

[8] M. Cappaci, G. Matticari, G. E. Noci, P. Siciliano, M. Berti, L. Biagoni, U. Cesari, E. Gengembre, and E. Chesta, in *40th AIAA Joint Propulsion Conference*, AIAA-2004-3771 (American Institute of Aeronautics and Astronautics, Reston, (Fort Lauderdale, FL, 2004).
[9] J. Perez-Luna, G. J. M. Hagelaar, L. Garrigues, and J. P. Boeuf, Phys. Plasmas 14, 113502 (2007).
[10] H. Kuwano, H. Nakashima, and H. Kuninaka, in *Proc. 24th Int. Symp. Space Technology and Science*, (Miyazaki, Japan, 2004), p. Paper ISTS 2004.
[11] L. Dubois, F. Gaboriau, L. Liard, D. Harribey, C. Henaux, L. Garrigues, G. J. H. Hagelaar, S. Mazouffre, C. Boniface, and J. P. Boeuf, Physics of Plasmas 25 093503 (2018).
[12] L. Dubois, F. Gaboriau, L. Liard, C. Boniface, and J. P. Boeuf, Physics of Plasmas 25 093504 (2018).
[13] L. Dubois, F. Gaboriau, L. Liard, D. Harribey, C. Henaux, S. Mazouffre, and C. Boniface, in *35th International Electric Propulsion Conference*, IEPC-2017-215, ( Atlanta, Ga, 2017).
[14] R. Joussot, L. Grimaud, S. Mazouffre, C. Boniface, S. Oriol, and F. Masson, in *The 5th Space Propulsion Conference*, (Roma, Italy, 2016), p. SP2016.
[15] L. Dubois, PhD Thesis, University of Toulouse, 2018.
[16] A. Leufroy, T. Gibert, and A. Bouchoule, in *31st International Electric Propulsion Conference*, IEPC-2009-083 (Ann Arbor, Michigan, 2009).
[17] Y. Raitses, T. Moeller, and J. Szabo, in *30th International Electric Propulsion Conference*, IEPC-2007- 334, (Florence, Italy, 2007).
[18] D. Brown and A. D. Gallimore, in *31st International Electric Propulsion Conference*, IEPC 2009-030, (Ann Arbor, Michigan, 2009).
[19] F. Diop, T. Gibert, and A. Bouchoule, Phys. Plasmas 26, 063508 (2019).
[20] N. Gascon, M. Dudeck, and S. Barral, Phys. Plasmas 10, 4123 (2003).
[21] A. Gugliemi, A. Martin Ortega, F. Gaboriau, J. P. Boeuf, and C. Boniface, in *36th International Electric Propulsion Conference*, IEPC-2019-632, (University of Vienna, Vienna, Austria, 2019).
[22] HALLIS, Software: https://www.hallis-model.com
[23] V. A. Godyak, Plasma Sources Science and Technology 20, 025004 (2011).